KDM7 is a dual demethylase for histone H3 Lys 9 and Lys 27 and functions in brain development

Yu-ichi Tsukada, Tohru Ishitani and Keiichi I. Nakayama

Genes Dev. 2010 24: 432-437
Access the most recent version at doi:10.1101/gad.1864410

RESEARCH COMMUNICATION

KDM7 is a dual demethylase for histone H3 Lys 9 and Lys 27 and functions in brain development

Yu-ichi Tsukada,[1,2,3] Tohru Ishitani,[4] and Keiichi I. Nakayama[1,2,5]

[1]Division of Cell Biology, Medical Institute of Bioregulation, Kyushu University, Higashi-ku, Fukuoka 812-8582, Japan; [2]CREST, Japan Science and Technology Agency (JST), Kawaguchi, Saitama 332-0012, Japan; [3]PRESTO, Japan Science and Technology Agency (JST), Kawaguchi, Saitama 332-0012, Japan; [4]Division of Cell Regulation Systems, Medical Institute of Bioregulation, Kyushu University, Higashi-ku, Fukuoka 812-8582, Japan

Methylation of histone H3 Lys 9 and Lys 27 (H3K9 and H3K27) is associated with transcriptional silencing. Here we show that KDM7, a JmjC domain-containing protein, catalyzes demethylation of both mono- or dimethylated H3K9 and H3K27. Inhibition of KDM7 orthologs in zebrafish resulted in developmental brain defects. KDM7 interacts with the follistatin gene locus, and KDM7 depletion in mammalian neuronal cells suppressed follistatin gene transcription in association with increased levels of dimethylated H3K9 and H3K27. Our findings identify KDM7 as a dual demethylase for H3K9 and H3K27 that functions as an eraser of silencing marks on chromatin during brain development.

Supplemental material is available at http://www.genesdev.org.

Received September 16, 2009; revised version accepted December 31, 2009.

Histone methylation status defines the epigenetic program of a cell by determining chromatin structure and thereby regulating DNA-dependent processes such as transcription (Strahl and Allis 2000; Lachner et al. 2003; Margueron et al. 2005; Martin and Zhang 2005). Histone methylation has also been linked to regulation of neuronal function (Iwase et al. 2007). The recent discovery of histone demethylases revealed that histone methylation is a more dynamic process than previously recognized, and that most identified demethylases show a strict substrate specificity limited to a single methylation site (Bannister et al. 2002; Shi et al. 2004; Klose et al. 2006a; Tsukada et al. 2006; Shi and Whetstine 2007; Cloos et al. 2008; Lan et al. 2008). A number of histone demethylases contain a JmjC domain, and a subfamily of JmjC domain-containing proteins (comprising KIAA1718, PHF8, and PHF2) is evolutionarily conserved from *Caenorhabditis elegans* to humans and is characterized by the presence of a PHD-type zinc finger motif in addition to the JmjC domain (Supplemental Fig. S1A). Whereas the human genes for PHF8 and PHF2 are associated with X-linked mental retardation and hereditary sensory neuropathy type I, respectively (Hasenpusch-Theil et al. 1999; Laumonnier et al. 2005; Abidi et al. 2007; Koivisto et al. 2007), little is known about KIAA1718. Bioinformatic analysis of the JmjC domains of KIAA1718, PHF8, and PHF2 indicated that predicted Fe(II)- and α-ketoglutarate (α-KG)-binding sites are conserved, with the exception of the former in PHF2, and that they share extensive similarity with the JmjC domain of JHDM1/KDM2 (Supplemental Fig. S1B). Conservation of residues within the putative cofactor-binding sites of KIAA1718 suggested that this protein might possess histone demethylase activity, and therefore might also contribute to transcriptional regulation of genes in the nervous system.

[*Keywords*: Demethylase; JmjC; methylation; histone; chromatin; epigenetics]

[5]Corresponding author.
E-MAIL nakayak1@bioreg.kyushu-u.ac.jp; FAX 81-92-642-6819.

Article is online at http://www.genesdev.org/cgi/doi/10.1101/gad.1864410.

Results and Discussion

KIAA1718 possesses histone demethylase activity

To examine whether KIAA1718 indeed possesses histone demethylase activity, we generated the mouse protein tagged with the Flag epitope at its C terminus in insect cells (Fig. 1A), and incubated the recombinant protein with histone substrates labeled with ^{3}H at various characterized methyl-lysine or methyl-arginine sites by corresponding histone methyltransferases (HMTs). Histone demethylase activity was monitored by measurement of the release of the labeled demethylation product, formaldehyde. Substantial release of labeled formaldehyde was observed in the reaction mixture containing histone H3 labeled on Lys 9 (H3K9) by G9a, but not in those containing histone substrates modified by other HMTs (Fig. 1B). Consistent with the notion that the observed enzymatic activity was intrinsic to KIAA1718, formaldehyde release from G9a-labeled H3 was dependent on KIAA1718 concentration (Fig. 1C). To ascertain whether the demethylation mediated by KIAA1718 is oxidative in nature, with Fe(II) and α-KG as cofactors, we examined whether the enzymatic activity of KIAA1718 is dependent on these cofactors. The release of formaldehyde mediated by KIAA1718 was indeed found to require both Fe(II) and α-KG (Fig. 1D). Ascorbate was also required for the enzymatic activity, presumably as a result of its ability to regenerate Fe(II) from Fe(III). To verify further that the observed enzymatic activity is attributable to a genuine demethylase, we generated recombinant forms of KIAA1718 that either lack the JmjC or PHD domains or contain a mutation (H282A) in the Fe(II)-binding site in insect cells (Fig. 1E). Analysis of similar amounts of the mutant proteins for histone demethylase activity revealed that deletion of the JmjC domain or mutation of His^{282} abolished the activity of KIAA1718, whereas the PHD domain appeared to be dispensable for such activity (Fig. 1E,F). Together, these results showed that KIAA1718 is a histone demethylase capable of removing methyl groups from H3K9. Given that histone demethylase activity is the first function attributed to KIAA1718, we named this protein KDM7 on the basis of the previously described nomenclature (Allis et al. 2007).

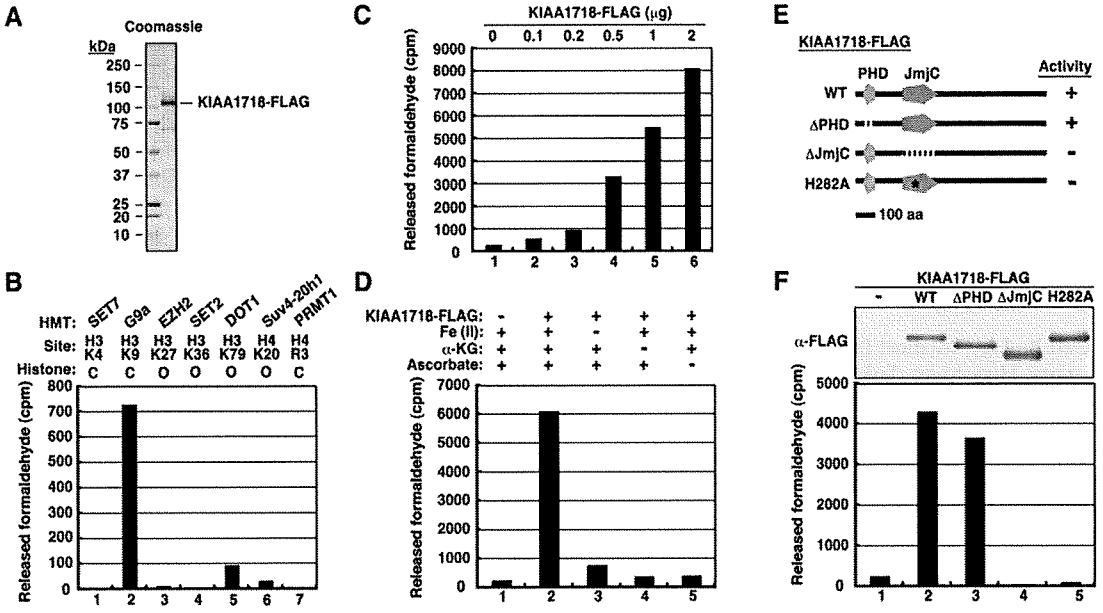

Figure 1. KIAA1718 is a histone demethylase that targets H3K9. (*A*, *right* lane) SDS–polyacrylamide gel electrophoresis with Coomassie blue staining of a C-terminally Flag-tagged recombinant KIAA1718 protein. Molecular size standards are shown in the *left* lane. (*B*) Histone demethylase activity of purified KIAA1718-Flag with various methylated histone substrates. The HMTs used to generate the various substrates and their sites of methylation are indicated. The methylated substrates were generated with the indicated forms of histone ([C] core histone octamer; [O] oligonucleosome) on the basis of the substrate preference of each HMT. The presented counts have been corrected for control counts. (*C*) Histone demethylase activity of the indicated amounts of KIAA1718-Flag. (*D*) Effects of removal of Fe(II), α-KG, or ascorbate from the reaction mixture on the histone demethylase activity of KIAA1718-Flag with G9a-methylated histone substrate. (*E*) Schematic representation of wild-type (WT) and mutant forms of KIAA1718 showing whether they are active (+) or inactive (−) as H3K9 demethylases. (*F*, *bottom* panel) Demethylase activity of purified wild-type or mutant forms of KIAA1718-Flag with G9a-methylated histone substrate. (*Top* panel) The similar amounts of KIAA1718-Flag proteins used in the demethylase assay are revealed by immunoblot analysis with antibodies to Flag (α-Flag).

KDM7 is a dual demethylase for dimethylated and monomethylated H3K9 (H3K9me2/me1) and H3K27me2/me1

To define the substrate and modification state specificity of KDM7, we included core histones as substrates in demethylation reaction mixtures and examined the modification status of individual methylation sites by immunoblot analysis with a series of methylation-specific antibodies. Wild-type KDM7 mediated a marked decrease in the methylation level of both H3K9me2 and H3K27me2, without affecting that of other histone methylation sites (Fig. 2A; Supplemental Fig. S2A). In addition, KDM7 efficiently removed methyl groups from H3K9me2 and H3K27me2 in core histones, but not from those in mono- or oligonucleosomes (Supplemental Fig. S2B,C). These results suggested that KDM7 prefers core histones rather than mono- or oligonucleosomes as substrates, and explain why demethylase activity was not detected by the radioactive formaldehyde release assay with nucleosomal histones methylated by the HMT EZH2 (Fig. 1B). They also suggested that the low level of reactivity apparent in the formaldehyde release assay with oligonucleosomes modified by DOT1 or Suv4-20h1 as substrates does not reflect demethylase activity of KDM7. To refine further the specificity of KDM7, we used methylated peptides as substrates in demethylation reactions and analyzed the removal of methyl groups from the peptides by mass spectrometry. This assay showed that KDM7 removed methyl groups from both H3K9me2 and H3K27me2 (Fig. 2B,C), eliminating the possibility of cross-reaction of antibodies between methylated H3K9 and H3K27 in the immunoblot analysis. KDM7 also demethylated both H3K9me1 and H3K27me1 (Fig. 2B,C), activity that was not apparent by immunoblot analysis (Fig. 2A), probably because demethylation by KDM7 is not highly processive, so that a reduction in the level of monomethylation is masked by production of monomethylated histone from dimethylated histone in a reaction with core histones that contain all three states of methylation, as compared with peptides containing a single monomethylation state. No demethylation was detected with trimethylated H3K9 (H3K9me3) or H3K27me3 peptides. A low level of demethylation activity was also apparent with an H3K36me2 peptide, but no demethylation of H3K36me1 or H3K36me3 was detected (Fig. 2D). The decrease in mass corresponding to a methyl group was not detected in reaction mixtures containing other methylated histone peptides (Supplemental Fig. S3). Together, these data suggested that KDM7 is an authentic histone demethylase with the ability to mediate the direct removal of methyl groups from H3K9me2/me1 and H3K27me2/me1.

Zebrafish KDM7 orthologs possess histone demethylase activity for H3K9/K27 and are expressed predominantly in the brain

To explore the biological function of KDM7 in vivo, we characterized the KDM7 orthologs in zebrafish—LOC321248 and LOC558416, hereafter designated drKDM7a and drKDM7b, respectively (Supplemental Fig. S1A)—both of which were also found to manifest histone demethylase activity toward H3K9me2 and

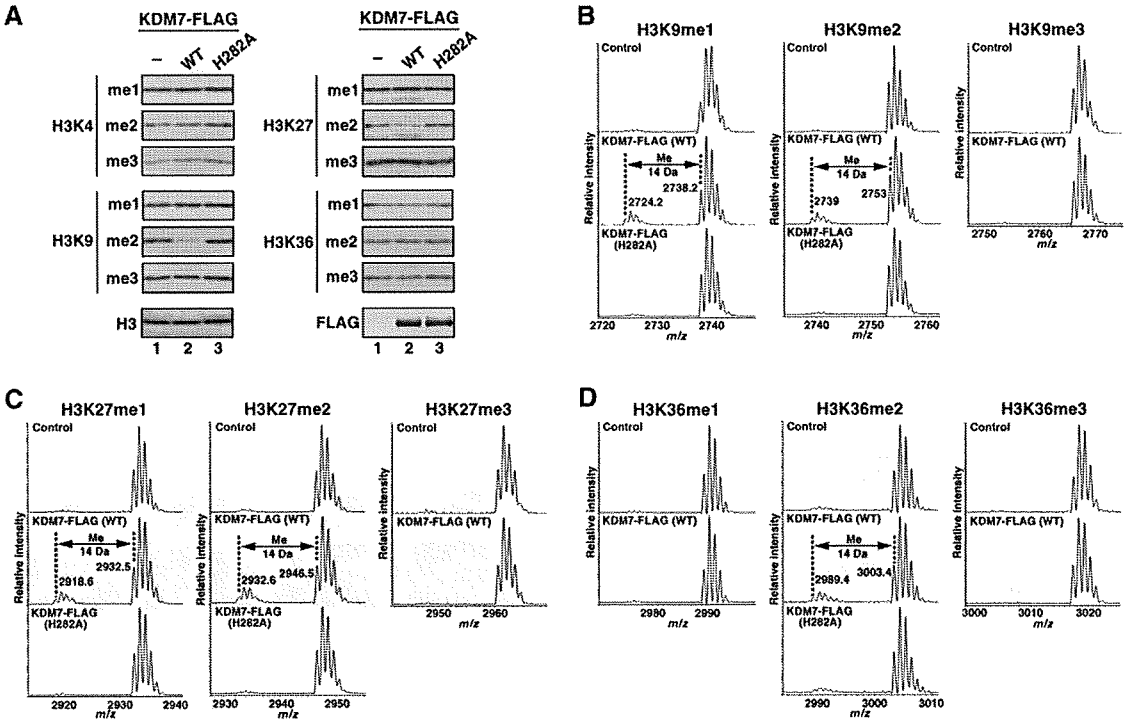

Figure 2. KDM7 is a histone demethylase specific for dimethylated or monomethylated H3K9 or H3K27. (*A*) Calf thymus core histones were incubated in the absence or presence of 5 μg of wild-type or H282A mutant forms of KDM7-Flag, after which histone demethylation was evaluated by immunoblot analysis with antibodies to specific modified histones, as indicated on the *left*. (*B–D*) Mass spectrometric analysis of the demethylase activity of 4 μg of wild-type or H282A mutant forms of KDM7-Flag with methylated H3K9, H3K27, or H3K36 peptide substrates. Numbers represent the masses of the peptide substrates and products.

H3K27me2 in core histones (Supplemental Fig. S4A). We first examined the expression patterns of *kdm7a* and *kdm7b* during development by in situ hybridization. Transcripts corresponding to *kdm7a* and *kdm7b* were detected as early as the post-somitogenesis stage at 24 h post-fertilization (hpf) in the brain and tail bud (Fig. 3A,B), whereas no signals were observed in embryos at 6 or 12 hpf (data not shown). The expression of both *kdm7* genes became prominent in the tectum, hindbrain, fin bud, and gill at 48 hpf (Fig. 3A,B). Corresponding sense probes did not yield any signals at these various stages of development (Supplemental Fig. S4B), indicating that the signals attributed to *kdm7* transcripts were specific.

Zebrafish KDM7 orthologs are required for tectum development

Given that both *kdm7* genes are expressed predominantly in the brain, we examined whether drKDM7 might function in brain development. To examine this possibility, we inhibited the function of drKDM7 with the use of two splicing-blocking antisense morpholino oligonucleotides (MOs) that independently target *kdm7a* or *kdm7b*. We also studied the stable transgenic line Tg(*HuC:Kaede*), which expresses the fluorescent protein Kaede in neurons under the control of the vertebrate neuron-specific promoter of the *HuC* gene, in order to visualize neurons (Sato et al. 2006). The level of mature mRNAs derived from the two *kdm7* genes was reduced specifically in embryos injected with the corresponding MO, but not in those injected with a control MO (Supplemental Fig. S5A). At 48 hpf, embryos that had been subjected to simultaneous injection of both *kdm7* MOs at the one-cell stage manifested a curly tail and marked decrease in size of the tectum (Fig. 3C,D), consistent with the observed expression of *kdm7* in the brain and tail bud. Importantly, the reduction in tectum size was accompanied by the loss of neurons from this region, although neurons in the spinal cord and other regions of the brain were unaffected (Fig. 3D; Supplemental Fig. S5B,C). In contrast, injection of MOs specific for each *kdm7* gene alone elicited only marginal effects compared with those of the control MO, a finding likely attributable to functional redundancy of the two *kdm7* genes. The persistence at 72 hpf of the phenotypes of the embryos injected with both *Kdm7* MOs eliminates the possibility that they were attributable to developmental delay (Fig. 3C; Supplemental Fig. S5B,C). Embryos that had been subjected to simultaneous injection of another set of MOs that independently target *kdm7a* and *kdm7b* also manifested phenotypes (Supplemental Fig. S6) similar to those observed with the original set (Fig. 3C,D), suggesting that the phenotypes were the specific consequence of depletion of *kdm7* transcripts. Coinjection of a validated MO for p53 (Robu et al. 2007) with either of the two independent sets of MOs for *kdm7* did not affect the phenotypes induced by MO-mediated depletion of *kdm7* transcripts (Supplemental Fig. S7), eliminating the possibility that the phenotypes were the result of p53 activation. Given that the phenotypes were not attributable to cell death (Supplemental Fig. S8), drKDM7 might regulate the proliferation or differentiation of neurons. On

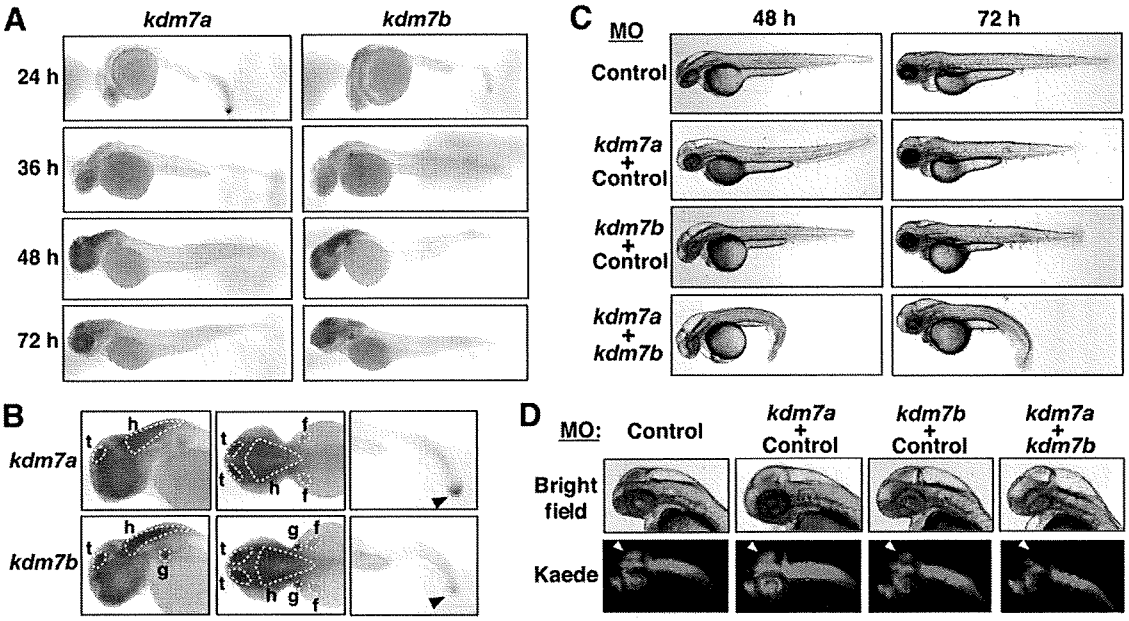

Figure 3. Zebrafish *kdm7* genes are expressed predominantly in brain and are required for tectum development. (*A*) In situ hybridization of whole-mount zebrafish embryos at the indicated stages (hpf) with antisense *kdm7a* or *kdm7b* RNA probes. (*B*) In situ hybridization of whole-mount embryos at 48 hpf (*left* and *middle* panels) or 24 hpf (*right* panels) with antisense *kdm7a* or *kdm7b* RNA probes. Lowercase letters indicate the tectum (t), hindbrain (h), fin bud (f), and gill (g). Arrowheads indicate the tail bud. (*C*) The Tg(*HuC:Kaede*) embryos were injected at the one-cell stage with antisense MOs for *kdm7a* (5 ng) or *kdm7b* (5 ng) or with a control MO (5 or 10 ng for a total of 10 ng of MO) in the indicated combinations. The morphology of the embryos at the indicated times (hpf) was examined by bright-field microscopy. (*D*) Morphology of the head region of embryos at 48 hpf that were injected with MOs as in *C*. (*Bottom* panels) Neurons expressing Kaede under the control of the HuC gene promoter were visualized by fluorescence microscopy. Arrowheads indicate the tectum or presumptive tectal region. Bright-field images are shown in the *top* panels.

the other hand, ectopic overexpression of a fragment of drKDM7a comprising amino acids 1–480 (which manifested demethylase activity similar to that of the full-length protein) achieved by mRNA injection at the one-cell stage resulted in severe developmental defects in zebrafish embryos (Supplemental Fig. S9), suggesting that spatially and temporally regulated expression of drKDM7 is necessary for proper development. Together, these results thus indicated that KDM7 plays an important role in brain development.

KDM7 directly regulates transcription and H3K9me2 and H3K27me2 levels of the follistatin gene

Quantitative RT–PCR analysis revealed that *Kdm7* mRNA was more abundant specifically in the cerebrum and cerebellum than in other mouse tissues, although low levels of *Kdm7* expression were apparent in a wide spectrum of tissues in the mouse (Supplemental Fig. S10A). To investigate the molecular basis for the abnormal brain development in zebrafish embryos depleted of drKDM7, as well as the function of KDM7 in neurons, we examined the effect of KDM7 depletion on the mRNA profile of the mouse neuroblastoma cell line Neuro2A, in which the abundance of KDM7 was found to be greater than that in other cell lines originating from various tissues (Supplemental Fig. S10B). To this end, we stably transfected Neuro2A cells with vectors for two shRNAs—KD1 and KD2—that target two different regions of mouse *Kdm7* mRNA. Quantitative RT–PCR and immunoblot analyses revealed that the amounts of *Kdm7* mRNA and KDM7 protein were markedly decreased in cells transfected with either of these vectors compared with those in parental cells or in cells transfected with a vector for a control shRNA (Fig. 4A,B). Microarray analysis of mRNAs in control cells and in those depleted of KDM7 resulted in the identification of genes whose expression was affected by KDM7 depletion (Supplemental Fig. S10C). One of these genes whose expression was markedly decreased by loss of KDM7 was that for follistatin, on which we initially focused, given that follistatin functions as an endogenous inhibitor of members of the transforming growth factor (TGF)-β superfamily, including activin, which plays an important role in brain development (Hemmati-Brivanlou et al. 1994; Lin et al. 2003; Zhu et al. 2008). We confirmed by quantitative RT–PCR analysis that the abundance of follistatin mRNA was decreased in Neuro2A cells depleted of KDM7 (Fig. 4C). Consistent with the results obtained with Neuro2A cells, depletion of KDM7 by RNAi in primary cultured mouse neurons also resulted in down-regulation of follistatin mRNA (Fig. 4D).

To determine whether the follistatin gene is a direct target of KDM7, we performed a series of chromatin immunoprecipitation (ChIP) experiments to examine its promoter and coding regions in Neuro2A cells (Fig. 4E). This analysis revealed the association of KDM7 with the follistatin gene, predominantly around the transcription start site (Fig. 4F). To investigate the consequences of this association, we analyzed H3K9me2 and H3K27me2 levels in the promoter and coding regions of the gene. Depletion of KDM7 resulted in an increase in both H3K9me2 and H3K27me2 levels around the transcription start site of the gene that appeared to correlate

with KDM7 occupancy (Fig. 4G). Depletion of KDM7 by RNAi in Neuro2A cells did not markedly affect H3K9me3 levels of the follistatin gene (Supplemental Fig. S11A). In contrast, depletion of KDM7 paradoxically increased H3K27me3 levels in the entire region of the gene (Supplemental Fig. S11B), although KDM7 showed no activity toward H3K27me3 in vitro. Given that the regions in which H3K27me3 levels were increased did not correlate with KDM7 occupancy, the observed changes in H3K27me3 levels were most likely an indirect effect of KDM7 depletion. These results suggested that the follistatin gene is a direct target of KDM7-mediated transcriptional activation.

We thus examined whether the zebrafish follistatin gene is dysregulated in *kdm7* morphants with the use of in situ hybridization. Whereas control morphants showed expression of the follistatin gene in an anterior edge region of the tectum at 48 hpf, *kdm7* morphants manifested a substantial decrease in such expression (Fig. 4H). The down-regulation of follistatin gene expression in this particular region was sustained at 60 and 72 hpf (Supplemental Fig. S12A). The corresponding sense probe did not yield any signals at the corresponding stages (Supplemental Fig. S12B). These results thus suggested that KDM7 is recruited to specific regions of the genome, and there functions as an H3K9 and H3K27 demethylase in vivo. To investigate whether follistatin contributes to brain development in zebrafish, we inhibited the function of follistatin with the use of two independent MOs that target the follistatin gene. At 48 hpf, embryos that had been injected with either *follistatin* MO at the one-cell stage manifested a loss of neurons from the tectum region, although neurons in the spinal cord and other regions of the brain were unaffected (Supplemental Fig. S13). Coinjection of the validated MO for p53 did not affect this phenotype (Fig. 4I; Supplemental Fig. S13C). Together, these results indicated that KDM7 contributes to brain development at least in part through regulation of follistatin gene expression.

Methylation of H3K9 and H3K27 is linked to formation of tightly packed chromatin (heterochromatin) and transcriptional silencing (Martin and Zhang 2005). We showed here that KDM7 is a histone demethylase that catalyzes demethylation at both H3K9 and H3K27. Among the JmjC domain-containing histone demethylases, only JHDM3/JMJD2 has been shown to act as a dual demethylase, targeting both H3K9 and H3K36 and functioning as a transcriptional repressor of the ASCL2 gene, although the consequence of simultaneous methylation of these sites remains unclear (Klose et al. 2006b; Whetstine et al. 2006). We therefore propose that KDM7 functions as an eraser of silencing marks on chromatin to unlock gene silencing. Consistent with this notion, we found that removal of methyl groups from H3K9 and H3K27 by KDM7 is associated with transcriptional activation of the follistatin gene. KDM7 belongs to the subfamily of JmjC domain-containing proteins composed of PHF2 and PHF8 in addition to KDM7. The expression of *Phf2* is concentrated in the embryonic neural tube and

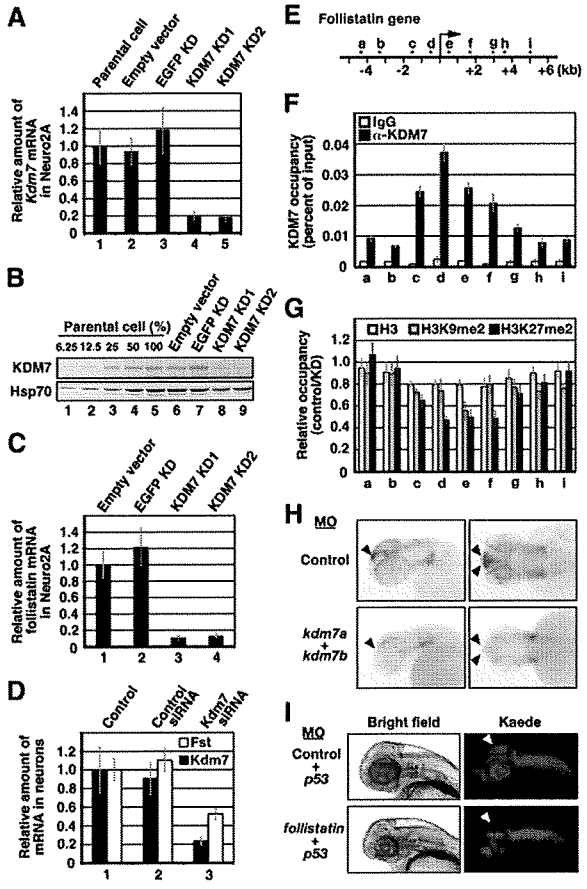

Figure 4. KDM7 directly regulates transcription and both H3K9me2 and H3K27me2 levels of the mouse follistatin gene. (*A*) Quantitative RT–PCR analysis of *Kdm7* mRNA in Neuro2A cell lines stably transfected with vectors for one of two KDM7 shRNAs (KD1 or KD2), with a vector for a control (EGFP) shRNA, or with the empty vector. The amount of *Kdm7* mRNA was normalized by that of *Gapdh* mRNA, and the normalized values are presented relative to that for the parental cells. Data are means ± SD. (*B*) Immunoblot analysis of KDM7 and Hsp70 (loading control) in the cell lines described in *A*. (*C*) Quantitative RT–PCR analysis of follistatin mRNA in the cell lines described in *A*. The amount of follistatin mRNA was normalized by that of *Gapdh* mRNA, and the normalized values are presented relative to that for the cells transfected with the empty vector. Data are means ± SD. (*D*) Quantitative RT–PCR analysis of *Kdm7* and follistatin (*Fst*) mRNAs in primary cultured mouse neurons treated with control or *Kdm7* siRNAs. The amounts of *Kdm7* and follistatin mRNAs were normalized by that of *Gapdh* mRNA, and the normalized values are presented relative to that for control cells. Data are means ± SD. (*E*) Schematic representation of the mouse follistatin genomic locus. The region from a to i was analyzed by ChIP experiments. The transcription start site is indicated by the arrow. (*F,G*) ChIP analysis of the relative occupancy of the sites in the follistatin genomic region indicated in *E* with KMD7 (*F*), as well as with H3 (white bars), H3K9me2 (gray bars), and H3K27me2 (black bars) (*G*). The analysis was performed with cells stably transfected with the vector for EGFP shRNA (control) and with cells stably expressing the KD1 shRNA for KDM7 (KD), and the results are presented as the percent of input for control cells (*F*) or the control/KD ratio (*G*). All data are means ± SD. (*H*) In situ hybridization of whole-mount zebrafish embryos at 48 hpf with an antisense follistatin RNA probe. Arrowheads indicate regions expressing the follistatin gene in embryos injected at the one-cell stage with antisense MOs for *kdm7a* (5 ng) and *kdm7b* (5 ng) or with a control MO (10 ng). (*I*) The Tg(*HuC:Kaede*) embryos were injected at the one-cell stage with antisense MOs for follistatin (5 ng) or p53 (5 ng) genes or with a control MO (5 ng) in the indicated combinations. The morphology of the embryos at 48 hpf was examined by bright-field (*left* panels) or fluorescence (*right* panels) microscopy. Arrowheads indicate the tectum or presumptive tectal region.

root ganglia in mice, and mutation of human *PHF8* causes inherited X-linked mental retardation (Hasenpusch-Theil et al. 1999; Laumonnier et al. 2005; Abidi et al. 2007; Koivisto et al. 2007). Our results showed that KDM7 is expressed predominantly in the brain of fish and mice as well as in mammalian neuronal cells and is essential for development of the fish brain, suggesting that transcriptional regulation of the follistatin gene by KDM7 may be evolutionarily conserved. Functions in neuronal development based on their demethylase activity may thus be common to this class of JmjC domain-containing proteins.

Materials and methods

In vitro histone demethylase assays

We performed in vitro demethylation assays with the use of purified recombinant proteins and various forms of histone substrates. Demethylase activity was detected by measurement of formaldehyde release, immunoblot analysis with a series of methylation-specific antibodies (Supplemental Table S1), or matrix-assisted laser desorption ionization (MALDI)–time-of-flight (TOF) mass spectrometry, as detailed in the Supplemental Material.

In situ hybridization

Whole-mount zebrafish embryos were subjected to in situ hybridization under standard conditions with digoxigenin-labeled antisense RNA probes prepared from zebrafish *kdm7a* (XM_687822), *kdm7b* (XM_681621), or follistatin 1 (DQ317968) genes.

Other methods

Details of other procedures are provided in the Supplemental Material.

Acknowledgments

We thank B.D. Strahl for providing pCAL-SpSet2, National BioResource Project ZEBRAFISH for providing *HuC:Kaede* transgenic fish, and members of our laboratories for discussion. This work was supported in part by a grant from the Ministry of Education, Culture, Sports, Science, and Technology of Japan.

References

Abidi FE, Miano MG, Murray JC, Schwartz CE. 2007. A novel mutation in the PHF8 gene is associated with X-linked mental retardation with cleft lip/cleft palate. *Clin Genet* **72:** 19–22.

Allis CD, Berger SL, Cote J, Dent S, Jenuwien T, Kouzarides T, Pillus L, Reinberg D, Shi Y, Shiekhattar R, et al. 2007. New nomenclature for chromatin-modifying enzymes. *Cell* **131:** 633–636.

Bannister AJ, Schneider R, Kouzarides T. 2002. Histone methylation: Dynamic or static? *Cell* **109:** 801–806.

Cloos PA, Christensen J, Agger K, Helin K. 2008. Erasing the methyl mark: Histone demethylases at the center of cellular differentiation and disease. *Genes & Dev* **22:** 1115–1140.

Hasenpusch-Theil K, Chadwick BP, Theil T, Heath SK, Wilkinson DG, Frischauf AM. 1999. PHF2, a novel PHD finger gene located on human chromosome 9q22. *Mamm Genome* **10:** 294–298.

Hemmati-Brivanlou A, Kelly OG, Melton DA. 1994. Follistatin, an antagonist of activin, is expressed in the Spemann organizer and displays direct neuralizing activity. *Cell* **77:** 283–295.

Iwase S, Lan F, Bayliss P, de la Torre-Ubieta L, Huarte M, Qi HH, Whetstine JR, Bonni A, Roberts TM, Shi Y. 2007. The X-linked mental retardation gene SMCX/JARID1C defines a family of histone H3 lysine 4 demethylases. *Cell* **128:** 1077–1088.

Klose RJ, Kallin EM, Zhang Y. 2006a. JmjC-domain-containing proteins and histone demethylation. *Nat Rev Genet* **7:** 715–727.

Klose RJ, Yamane K, Bae Y, Zhang D, Erdjument-Bromage H, Tempst P, Wong J, Zhang Y. 2006b. The transcriptional repressor JHDM3A demethylates trimethyl histone H3 lysine 9 and lysine 36. *Nature* **442:** 312–316.

Koivisto AM, Ala-Mello S, Lemmela S, Komu HA, Rautio J, Jarvela I. 2007. Screening of mutations in the PHF8 gene and identification of a novel mutation in a Finnish family with XLMR and cleft lip/cleft palate. *Clin Genet* **72:** 145–149.

Lachner M, O'Sullivan RJ, Jenuwein T. 2003. An epigenetic road map for histone lysine methylation. *J Cell Sci* **116:** 2117–2124.

Lan F, Nottke AC, Shi Y. 2008. Mechanisms involved in the regulation of histone lysine demethylases. *Curr Opin Cell Biol* **20:** 316–325.

Laumonnier F, Holbert S, Ronce N, Faravelli F, Lenzner S, Schwartz CE, Lespinasse J, Van Esch H, Lacombe D, Goizet C, et al. 2005. Mutations in PHF8 are associated with X linked mental retardation and cleft lip/cleft palate. *J Med Genet* **42:** 780–786.

Lin SY, Morrison JR, Phillips DJ, de Kretser DM. 2003. Regulation of ovarian function by the TGF-β superfamily and follistatin. *Reproduction* **126:** 133–148.

Margueron R, Trojer P, Reinberg D. 2005. The key to development: Interpreting the histone code? *Curr Opin Genet Dev* **15:** 163–176.

Martin C, Zhang Y. 2005. The diverse functions of histone lysine methylation. *Nat Rev Mol Cell Biol* **6:** 838–849.

Robu ME, Larson JD, Nasevicius A, Beiraghi S, Brenner C, Farber SA, Ekker SC. 2007. p53 activation by knockdown technologies. *PLoS Genet* **3:** e78. doi: 10.1371/journal.pgen.0030078.

Sato T, Takahoko M, Okamoto H. 2006. HuC:Kaede, a useful tool to label neural morphologies in networks in vivo. *Genesis* **44:** 136–142.

Shi Y, Whetstine JR. 2007. Dynamic regulation of histone lysine methylation by demethylases. *Mol Cell* **25:** 1–14.

Shi Y, Lan F, Matson C, Mulligan P, Whetstine JR, Cole PA, Casero RA, Shi Y. 2004. Histone demethylation mediated by the nuclear amine oxidase homolog LSD1. *Cell* **119:** 941–953.

Strahl BD, Allis CD. 2000. The language of covalent histone modifications. *Nature* **403:** 41–45.

Tsukada Y, Fang J, Erdjument-Bromage H, Warren ME, Borchers CH, Tempst P, Zhang Y. 2006. Histone demethylation by a family of JmjC domain-containing proteins. *Nature* **439:** 811–816.

Whetstine JR, Nottke A, Lan F, Huarte M, Smolikov S, Chen Z, Spooner E, Li E, Zhang G, Colaiacovo M, et al. 2006. Reversal of histone lysine trimethylation by the JMJD2 family of histone demethylases. *Cell* **125:** 467–481.

Zhu CC, Boone JQ, Jensen PA, Hanna S, Podemski L, Locke J, Doe CQ, O'Connor MB. 2008. *Drosophila* Activin- and the Activin-like product Dawdle function redundantly to regulate proliferation in the larval brain. *Development* **135:** 513–521.

ARTICLES

Skp2 targeting suppresses tumorigenesis by *Arf-p53*-independent cellular senescence

Hui-Kuan Lin[1,2,3], Zhenbang Chen[1,2,4]†, Guocan Wang[1,2,4]*, Caterina Nardella[1,2,4]*, Szu-Wei Lee[3]*, Chan-Hsin Chan[3], Wei-Lei Yang[3], Jing Wang[3], Ainara Egia[4], Keiichi I. Nakayama[5], Carlos Cordon-Cardo[2]†, Julie Teruya-Feldstein[2] & Pier Paolo Pandolfi[1,2,4]

Cellular senescence has been recently shown to have an important role in opposing tumour initiation and promotion. Senescence induced by oncogenes or by loss of tumour suppressor genes is thought to critically depend on induction of the $p19^{Arf}$–p53 pathway. The Skp2 E3-ubiquitin ligase can act as a proto-oncogene and its aberrant overexpression is frequently observed in human cancers. Here we show that although *Skp2* inactivation on its own does not induce cellular senescence, aberrant proto-oncogenic signals as well as inactivation of tumour suppressor genes do trigger a potent, tumour-suppressive senescence response in mice and cells devoid of *Skp2*. Notably, *Skp2* inactivation and oncogenic-stress-driven senescence neither elicit activation of the $p19^{Arf}$–p53 pathway nor DNA damage, but instead depend on Atf4, p27 and p21. We further demonstrate that genetic *Skp2* inactivation evokes cellular senescence even in oncogenic conditions in which the $p19^{Arf}$–p53 response is impaired, whereas a Skp2–SCF complex inhibitor can trigger cellular senescence in p53/Pten-deficient cells and tumour regression in preclinical studies. Our findings therefore provide proof-of-principle evidence that pharmacological inhibition of Skp2 may represent a general approach for cancer prevention and therapy.

Cellular senescence represents an irreversible form of cell-cycle arrest that can be triggered by a variety of insults. Induction of cellular senescence (for example, by oncogenic Ras) results in $p19^{Arf}$ (encoded by the *Ink4a/Arf* locus, also known as *Cdkn2a* locus) and p53 accumulation, which is critical for this senescence response. Recent studies suggest that cellular senescence can act as an important tumour-suppressive mechanism to restrict tumour development *in vivo*[1–7].

Inactivation of Pten functions is frequently observed in human cancers[8–10]. Although Pten negatively regulates cell proliferation and survival, we surprisingly discovered that acute *Pten* inactivation triggers the accumulation of $p19^{Arf}$–p53 and cellular senescence[2]. Concomitant inactivation of *p53* (also known as *Trp53* in mice, and *TP53* in humans) and *Pten* abrogates this senescence response, in turn promoting invasive and lethal prostate cancer[2]. Although these findings further underscore the critical importance of the cellular senescence *Arf-p53* failsafe pathway, the frequent loss or mutation of *ARF* or *P53* in human cancers would compromise the tumour-suppressive efficacy of this response, thereby limiting therapeutic potential.

Skp2 is a critical component of the Skp2–SCF complex, which acts as an E3 ligase to target p27 and other substrates for ubiquitylation and degradation[11,12]. Recent studies suggest that Skp2 may have oncogenic activity[13–16]. Notably, SKP2 overexpression is frequently observed in human cancer[11,12,17], strongly suggesting that SKP2 overexpression may contribute to tumorigenesis. *Skp2*-knockout mice are viable and fertile[18]. Hence, specific inactivation of *Skp2* may represent an appealing therapeutic modality. Here we show that *Skp2* inactivation profoundly restricts tumorigenesis by eliciting cellular senescence only in oncogenic conditions. Remarkably, this senescence response is triggered in a $p19^{Arf}$–p53-independent manner. Skp2 pharmacological inactivation may therefore represent a general approach towards a 'pro-senescence' therapy for cancer prevention and treatment.

Skp2 loss restores cellular senescence by Ras and E1A

Skp2 deficiency delays cell cycle progression[11,12]. We therefore asked whether *Skp2* deficiency would trigger cellular senescence. We isolated mouse embryonic fibroblasts (MEFs) from wild-type and $Skp2^{-/-}$ mice and determined cellular senescence in these cells by senescence-associated β-galactosidase (SA-β-gal) staining. Although $Skp2^{-/-}$ MEFs proliferated less than wild-type MEFs (Supplementary Fig. 1e)[11,12], cellular senescence in $Skp2^{-/-}$ MEFs was comparable to that in the wild-type MEFs (Supplementary Fig. 1a). In contrast, acute inactivation of *Pten* in MEFs markedly increased cellular senescence as previously reported (Supplementary Fig. 1a)[2]. Thus, *Skp2* deficiency by itself does not elicit cellular senescence.

Ectopic overexpression of proto-oncogenic Ras (Ras(G12V)) in MEFs elicits cellular senescence through the $p19^{Arf}$–p53 pathway[19,20]. Simultaneous co-expression of E1A and Ras in MEFs overcomes Ras-induced senescence by preventing activation of the $p19^{Arf}$–p53 pathway and resulting in oncogenic transformation[20]. Thus, E1A enables Ras to overcome the cellular senescence response. As Skp2 also cooperates with oncogenic Ras to induce cell transformation[13], it is conceivable that Skp2 might also display its oncogenic activity by antagonizing Ras-induced cellular senescence. On this basis, we tested whether endogenous Skp2 activity is required for cellular transformation induced by Ras and E1A. Although cellular senescence was not

[1]Cancer Biology and Genetics Program, [2]Department of Pathology, Sloan-Kettering Institute, Memorial Sloan-Kettering Cancer Center, 1275 York Avenue, New York, New York 10021, USA. [3]Department of Molecular and Cellular Oncology, The University of Texas M.D. Anderson Cancer Center, Houston, Texas 77030, USA. [4]Cancer Genetics Program, Beth Israel Deaconess Cancer Center and Department of Medicine, Beth Israel Deaconess Medical Center, Harvard Medical School, 330 Brookline Avenue, Boston, Massachusetts 02215, USA. [5]Department of Molecular and Cellular Biology, Medical Institute of Bioregulation, Kyushu University, Fukuoka, Fukuoka 812-8582, Japan. †Present addresses: Department of Biochemistry and Cancer Biology, Meharry Medical College, 1005 Dr D. B. Todd Jr Boulevard, Nashville, Tennessee 37208-3599, USA (Z.C.); Irving Cancer Research Center, Room 309, 1130 St. Nicholas Avenue, New York, New York 10032, USA (C.C.-C.).
*These authors contribute equally to this work.

105

observed in wild-type MEFs after Ras and E1A overexpression, *Skp2* deficiency triggered cellular senescence (Supplementary Fig. 1b, c). We also found that the ability of Ras to induce cellular senescence was far greater in $Skp2^{-/-}$ MEFs than in wild-type MEFs (Supplementary Fig. 1b, c). It should be noted that the induction of $p19^{Arf}$ and p53 protein levels in $Skp2^{-/-}$ MEFs by Ras was comparable if not lower than that of wild-type MEFs (Supplementary Fig. 1d). Moreover, *Skp2* inactivation profoundly restricted cell proliferation and transformation after Ras and E1A overexpression (Supplementary Fig. 1e, f). Thus, *Skp2* inactivation triggers cellular senescence in the presence of powerful oncogenic signals, even when the $p19^{Arf}$–p53 response is evaded.

Skp2 loss causes senescence in $Pten^{+/-}$ and $Arf^{-/-}$ mutants

We assessed whether *Skp2* inactivation would trigger cellular senescence even when cells experience loss of major tumour-suppressive networks such as those controlled by Pten and $p19^{Arf}$–p53. To this end, we crossed $Skp2^{-/-}$ mutants with $Pten^{+/-}$ and $Arf^{-/-}$ mutants. The resulting compound mice were further intercrossed to generate MEFs of different genotypes for cell proliferation and senescence assays. As aforementioned, $Skp2^{-/-}$ MEFs grew much slower than wild-type MEFs, whereas wild-type and $Pten^{+/-}$ MEFs grew comparably (Supplementary Fig. 2a). No obvious cellular senescence was observed in wild-type, $Pten^{+/-}$ and $Skp2^{-/-}$ MEFs (Fig. 1a). Surprisingly, $Pten^{+/-}$ $Skp2^{-/-}$ MEFs had a slower growth rate than $Skp2^{-/-}$ MEFs and exhibited full-blown characteristics of cellular senescence such as flattened large cells and positive SA-β-gal staining (Fig. 1a and Supplementary Fig. 2a). We also detected cellular senescence in $Pten^{+/-}$ $Skp2^{-/-}$ MEFs under hypoxic conditions (Supplementary Fig. 2b). We did not see cooperation between *Pten* inactivation and *Skp2* deficiency in triggering apoptosis, although $Skp2^{-/-}$ MEFs had a higher rate of apoptosis than wild-type MEFs (Supplementary Fig. 3a)[18]. However, the apoptosis rate in the prostate of $Pten^{+/-}$ $Skp2^{-/-}$ mice was higher than in wild-type, $Pten^{+/-}$ and $Skp2^{-/-}$ mice (see later and Supplementary Fig. 3b).

As cellular senescence is largely dependent on activation of the $p19^{Arf}$–p53 pathway in MEFs[2,21,22], we determined whether this pathway is activated in $Pten^{+/-}$ $Skp2^{-/-}$ MEFs. Notably, we found that $p19^{Arf}$ and p53 protein levels in $Pten^{+/-}$ $Skp2^{-/-}$ MEFs were comparable to levels in wild-type MEFs (Fig. 1b and Supplementary Fig. 4), suggesting that the $p19^{Arf}$–p53 pathway may not be involved in the senescence response in $Pten^{+/-}$ $Skp2^{-/-}$ MEFs. To test this hypothesis further, we exposed MEFs of various genotypes to two well-established p53-inactivating tools: a short hairpin RNA (shRNA) against *p53* (ref. 23) or a dominant-negative p53 mutant (p53-DN)[24]. Notably, in both conditions cell growth was promoted in wild-type and $Pten^{-/-}$ MEFs (Supplementary Fig. 5a, b), but neither of them overcame the cellular senescence nor the growth arrest in $Pten^{+/-}$ $Skp2^{-/-}$ MEFs (Fig. 1c and Supplementary Fig. 5c), suggesting that *Skp2*-deficiency cooperates with *Pten* inactivation to trigger a new senescence response by a $p19^{Arf}$–p53-independent pathway.

$p19^{Arf}$ induction is required for cellular senescence in MEFs in the context of acute *Pten* inactivation[25], whereas loss of $p19^{Arf}$ leads to cell immortalization[2,21,22]. We investigated whether *Skp2* inactivation could elicit cellular senescence in an *Arf*-deficient genetic background. Notably, $Arf^{-/-}$ $Skp2^{-/-}$ MEFs showed massive cellular senescence similar to $Pten^{+/-}$ $Skp2^{-/-}$ MEFs (Fig. 1d). Moreover, p53 expression was not induced in $Arf^{-/-}$ $Skp2^{-/-}$ MEFs (Supplementary Fig. 6a). This cellular senescence profoundly suppressed the growth of $Arf^{-/-}$ MEFs (Supplementary Fig. 6b). *Skp2* deficiency also induced cellular senescence after p53 inactivation (Supplementary Fig. 6c, d).

DNA damage has been recently associated with cellular senescence[26–28]. However, we found no evidence of DNA-damage-response activation in $Pten^{+/-}$ $Skp2^{-/-}$ MEFs, as determined by the levels of phosphorylated-(S15)-p53 and -γ-H2ax (also known as γ-H2afx) (Supplementary Fig. 4). Collectively, these results support the notion that *Skp2* inactivation can trigger a new type of cellular senescence that does not involve DNA damage and can suppress transformation even when the $p19^{Arf}$–p53 response is impaired.

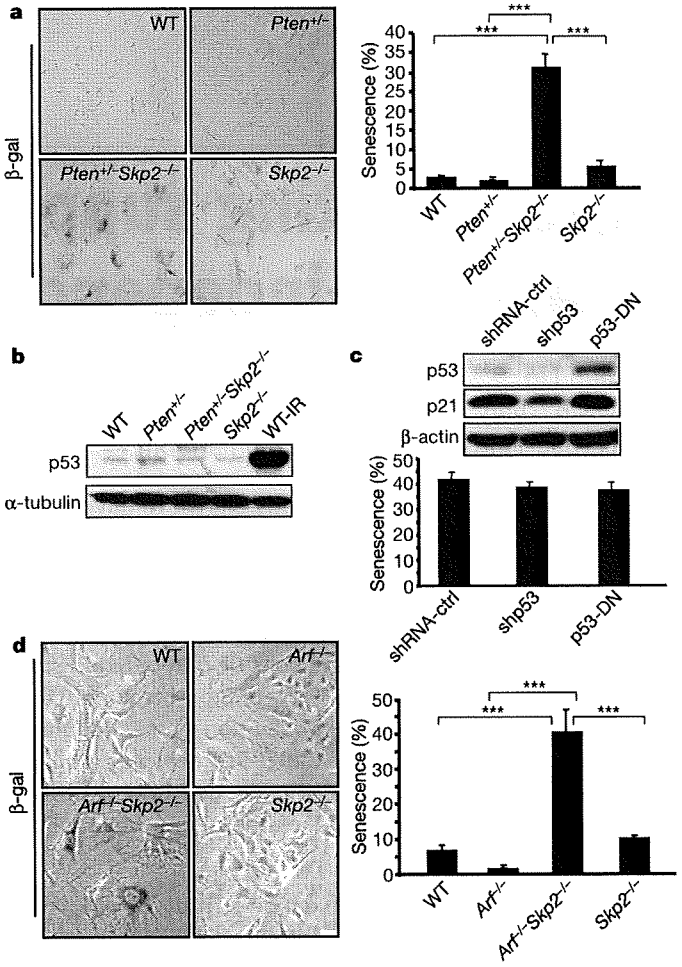

Figure 1 | *Skp2* loss triggers a new senescence response in MEFs in the context of *Pten* inactivation and *Arf* deficiency by a $p19^{Arf}$–p53-independent pathway. **a**, Primary MEFs at passage 5 from various mouse embryos were plated for senescence assay. WT, wild type. **b**, Cell lysates were collected from primary MEFs of various genotypes of mouse embryos for western blot analysis. The lysates from wild-type MEFs treated with γ-irradiation for 60 min served as a positive control for p53. **c**, Primary $Pten^{+/-}$ $Skp2^{-/-}$ MEFs infected with retroviruses expressing various control shRNA (shRNA-ctrl), *p53* shRNA (shp53), or dominant-negative p53 (p53-DN) were plated for senescence assay and western blot analysis. **d**, Primary MEFs at passage 5 from various genotypes of mouse embryos were plated for senescence assay. Results are presented as mean ± s.d. from a representative experiment performed in triplicate. $***P < 0.001$ using two-tailed Student's *t*-test, $n = 3$.

p27, p21 and Atf4 induction contribute to senescence

We next examined the molecular mechanism by which *Skp2* deficiency synergizes with oncogenic insults to trigger cellular senescence. Although p53 and $p19^{Arf}$ levels remained unchanged, we found that *Skp2* deficiency cooperated with *Pten* inactivation or *Arf* loss to induce p27 expression (Fig. 2a, b). p21 expression was also increased in $Pten^{+/-}$ $Skp2^{-/-}$ and $Arf^{-/-}$ $Skp2^{-/-}$ MEFs (Fig. 2a, b). E2F1, cyclin D1 and Cdt1, involved in cell cycle progression and DNA replication, are also targets for Skp2 (refs 12, 29). We found that cyclin D1, but not E2F1 and Cdt1, were induced in $Pten^{+/-}$ $Skp2^{-/-}$ MEFs (Supplementary Fig. 7a). Because cyclin D1 promotes cell cycle progression, its upregulation is unlikely to be involved in mediating senescence in $Pten^{+/-}$ $Skp2^{-/-}$ MEFs.

Endoplasmic reticulum (ER) stress proteins such as BiP (also known as Hspa5 or GRP78), phospho-Perk (p-Perk), and Atf4 are induced after oncogenic insults and have an important role in cellular

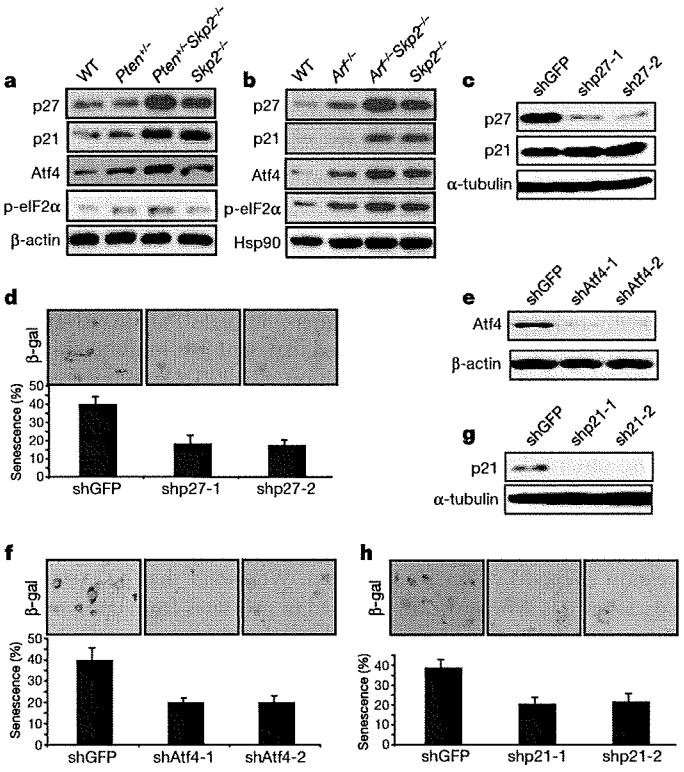

Figure 2 | Upregulation of p27, p21 and Atf4 drives cellular senescence in *Pten*$^{+/-}$ *Skp2*$^{-/-}$ and *Arf*$^{-/-}$ *Skp2*$^{-/-}$ MEFs. **a, b,** Cell lysates were collected from primary MEFs of various genotypes of mouse embryos for western blot analysis. **c, d,** *Pten*$^{+/-}$ *Skp2*$^{-/-}$ MEFs at passage 2 infected with lentiviruses expressing green fluorescent protein (GFP) shRNA (shGFP) or *p27* shRNA (shp27-1 and -2) were plated for western blot analysis (**c**) and senescence assay (**d**). Results are mean ± s.d. from a representative experiment performed in triplicate. **e, f,** *Pten*$^{+/-}$ *Skp2*$^{-/-}$ MEFs at passage 2 infected with lentiviruses expressing GFP shRNA or *Atf4* shRNA were plated for western blot analysis (**e**) and senescence assay (**f**). **g, h,** *Pten*$^{+/-}$ *Skp2*$^{-/-}$ MEFs at passage 2 infected with lentiviruses expressing GFP shRNA or *p21* shRNA were plated for western blot analysis (**g**) and senescence assay (**h**).

senescence[30]. We did not find a significant increase in BiP or p-Perk (Supplementary Fig. 7b and data not shown) in *Pten*$^{+/-}$ *Skp2*$^{-/-}$ MEFs. In contrast, Atf4 was markedly induced in *Pten*$^{+/-}$ *Skp2*$^{-/-}$ MEFs (Fig. 2a). Likewise, we also observed a marked increase in Atf4 protein levels, but not p-Perk, in *Arf*$^{-/-}$ *Skp2*$^{-/-}$ MEFs (Fig. 2b and Supplementary Fig. 7c). The induction of Atf4 protein levels in *Pten*$^{+/-}$ *Skp2*$^{-/-}$ MEFs was not accompanied by messenger RNA upregulation, nor by the enhanced Atf4 protein stability (Supplementary Fig. 8 and data not shown). Instead, we observed an increase in phosphorylated eIF2α (p-eIF2α; also known as p-Eif2s1) in *Pten*$^{+/-}$ *Skp2*$^{-/-}$ and *Arf*$^{-/-}$ *Skp2*$^{-/-}$ MEFs compared to wild-type cells (Fig. 2a, b). Because p-eIF2α positively regulates Atf4 translation[31], our results indicate that Atf4 upregulation is probably triggered by the enhancement of p-eIF2α levels.

As p27, p21 and Atf4 were induced in both *Pten*$^{+/-}$ *Skp2*$^{-/-}$ and *Arf*$^{-/-}$ *Skp2*$^{-/-}$ MEFs, we next determined whether their upregulation contributes to senescence. *p27* (also known as *Cdkn1b*) shRNA efficiently abrogated p27 expression and partially rescued growth arrest and cellular senescence in *Pten*$^{+/-}$ *Skp2*$^{-/-}$ MEFs (Fig. 2c, d and Supplementary Figs 9a, b and 10a). Similarly, knockdown of *Atf4* or *p21* (also known as *Cdkn1a*) in these cells also partially reversed cellular senescence and cell arrest (Fig. 2e–h and Supplementary Figs 9c and 10b, c). Concomitant knockdown of *Atf4*, *p21* and *p27* in these cells reversed cellular senescence more efficiently than their individual knockdown (Supplementary Fig. 10d). In contrast, in *Skp2*$^{-/-}$ MEFs, *p27* knockdown accelerated growth whereas *Atf4* knockdown did not (Supplementary Fig. 10e, f). These results strongly indicate that the concomitant upregulation of p27, p21and Atf4 is a required and powerful engine for the induction of cellular senescence upon *Skp2* inactivation.

Skp2 loss restricts tumorigenesis independently of *Arf-p53*

We found that inactivation of *Skp2* in the presence of an oncogenic stress results in the induction of cellular senescence that opposes transformation *in vitro* even when the p19^{Arf}–p53 response is impaired. We next determined whether *Skp2* loss restricts tumorigenesis *in vivo* through similar mechanisms, and first analysed tumorigenesis in *Skp2*$^{-/-}$ *Pten*$^{+/-}$ compound mutants (Supplementary Fig. 11a). Although *Pten* heterozygous inactivation reduced lifespan in mice, compound *Skp2* deficiency prolonged overall survival (Fig. 3a). *Pten*$^{+/-}$ mice develop lymphadenopathy and adrenal tumours (pheochromacytoma) at complete penetrance[32,33]. As expected, *Pten*$^{+/-}$ mice developed adrenal tumours with 100% penetrance by 1 year of age, whereas *Skp2* loss remarkably abrogated adrenal tumour formation in compound mutants ($P < 0.0001$; Fig. 3b, top, c and Supplementary Fig. 11b). Pten protein expression in adrenal tissues was comparable between wild-type, *Pten*$^{+/-}$ and *Pten*$^{+/-}$ *Skp2*$^{-/-}$ mice, before or after tumour occurrence, suggesting that there is no loss of heterozygosity at the *Pten* locus in the adrenal tissues in any of these mutants and conditions (Supplementary Fig. 11c). Lymphadenopathy after *Pten* inactivation was also profoundly inhibited by *Skp2* loss ($P < 0.01$; Fig. 3b,

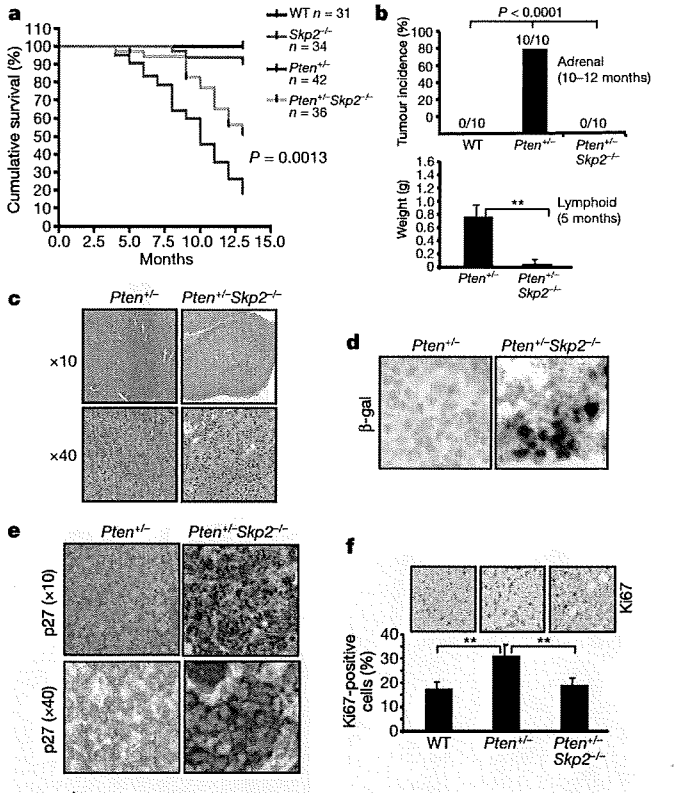

Figure 3 | *Skp2* deficiency restricts tumorigenesis after *Pten* inactivation by inducing cellular senescence *in vivo*. **a,** Kaplan–Meier plot analysis of cumulative survival of indicated mouse genotypes. **b,** Top, adrenal tissues from various mouse genotypes (10–12 months) were analysed for tumorigenesis; bottom, lymphoid tissues within the neck were obtained and weighed from female mice of various genotypes (around 5 months). $^{**}P < 0.01$ using two-tailed Student's *t*-test, $n = 6$. **c,** Histological analysis of adrenal tissues from 12-month-old *Pten*$^{+/-}$ and *Pten*$^{+/-}$ *Skp2*$^{-/-}$ mice. *Pten*$^{+/-}$ mice developed adrenal tumour (pheochromocytoma), which was profoundly inhibited in *Pten*$^{+/-}$ *Skp2*$^{-/-}$ mice. **d,** Senescence analysis of lymphoid tissue from 5-month-old *Pten*$^{+/-}$ and *Pten*$^{+/-}$ *Skp2*$^{-/-}$ mice. **e,** Lymphoid tissues from 5-month-old mice of the indicated genotypes were obtained for p27 immunohistochemistry. **f,** Quantification of Ki67 staining of lymphoid tissues from 5-month-old mice. Results are mean ± s.d. $^{**}P < 0.01$ using two-tailed Student's *t*-test, $n = 3$.

bottom and Supplementary Fig. 11d). Tumorigenesis was also markedly suppressed in other organs (for example, in the prostate, where the prostatic intraepithelial neoplasia (PIN) incidence was profoundly restricted by *Skp2* inactivation; data not shown).

To determine whether *Skp2* inactivation along with *Pten* inactivation would trigger cellular senescence *in vivo*, we performed SA-β-gal staining in the few hyperplastic lymphoid lesions still identified in $Pten^{+/-}$ $Skp2^{-/-}$ mice (see, for example, Supplementary Fig. 10d). We observed both cellular senescence and p27 induction in the lymphoid tissues from $Pten^{+/-}$ $Skp2^{-/-}$ mice (Fig. 3d, e and Supplementary Fig. 12), which inversely correlated with cell proliferation (Fig. 3f).

We then examined whether *Skp2* inactivation would also restrict tumorigenesis after *Arf* loss by crossing $Skp2^{-/-}$ with $Arf^{-/-}$ mice (Supplementary Fig. 13). *Skp2* inactivation markedly prolonged the overall survival of $Arf^{-/-}$ mice (Fig. 4a). Around 33% of $Arf^{-/-}$ mice developed sarcoma and/or lymphoma within 1 year (Fig. 4b–d)[34,35]. In contrast, none of the $Arf^{-/-}$ $Skp2^{-/-}$ compound mutant mice showed signs of tumour formation ($P < 0.02$; Fig. 4b–d).

Senescence after *Pten* and *Skp2* inactivation in the prostate

Complete *Pten* inactivation in the prostate triggers a tumour-suppressive cellular senescence response[2]. We therefore examined whether this response could be further potentiated by *Skp2* loss and affect tumorigenesis after complete *Pten* inactivation in the prostate. For prostate-specific inactivation, we made use of Cre-*loxP*-mediated recombination and probasin (*Pbsn*, also known as *PB*)-*Cre4* transgenic mice expressing the Cre recombinase after puberty in the prostatic epithelium[2]. We obtained $Pten^{loxP/loxP}$;*PB-Cre4* and $Pten^{loxP/loxP}Skp2^{-/-}$;*PB-Cre4* compound mutant mice, hereafter referred to as $Pten^{pc-/-}$ and $Pten^{pc-/-}$ $Skp2^{-/-}$ mice, respectively (Supplementary Fig. 14a). Although complete *Pten* inactivation in mouse prostates leads to invasive prostate cancers, it does not affect overall survival[2]. We did not detect a difference in overall survival between $Pten^{pc-/-}$ and $Pten^{pc-/-}$ $Skp2^{-/-}$ mice (Supplementary Fig. 14b).

Prostate cancer development in these mice was monitored by magnetic resonance imaging (MRI) and histopathological analysis. Consistent with our previous findings[2], MRI analysis showed prostate tumour masses in $Pten^{pc-/-}$ mice at 6 months of age, which were significantly reduced in $Pten^{pc-/-}$ $Skp2^{-/-}$ mice (Supplementary Fig. 14c). The average size of the prostate in $Pten^{pc-/-}$ mice was tenfold larger than in wild-type mice, whereas complete *Skp2* loss markedly reduced tumour weight after complete *Pten* inactivation (Fig. 5a). Histological analysis showed that *Skp2* loss inhibited invasive prostate cancer after *Pten* inactivation, albeit PIN lesions were still observed in $Pten^{pc-/-}$ $Skp2^{-/-}$ mice (Supplementary Fig. 14d, e). Furthermore, this suppressive effect by *Skp2* loss was persistent, as we also observed a profound reduction in tumour weight and invasive prostate cancer in $Pten^{pc-/-}$ $Skp2^{-/-}$ mice at 15 months of age (Supplementary Fig. 14f, g).

We next investigated, *in vivo*, the molecular basis for tumour suppression elicited by Skp2 inactivation. We found that p27 protein expression was synergistically induced in prostates from compound mutants, as determined by immunohistochemistry and western blot analysis (Supplementary Fig. 15a, b), whereas p53 expression was comparably induced in $Pten^{pc-/-}$ and $Pten^{pc-/-}$ $Skp2^{-/-}$ mice

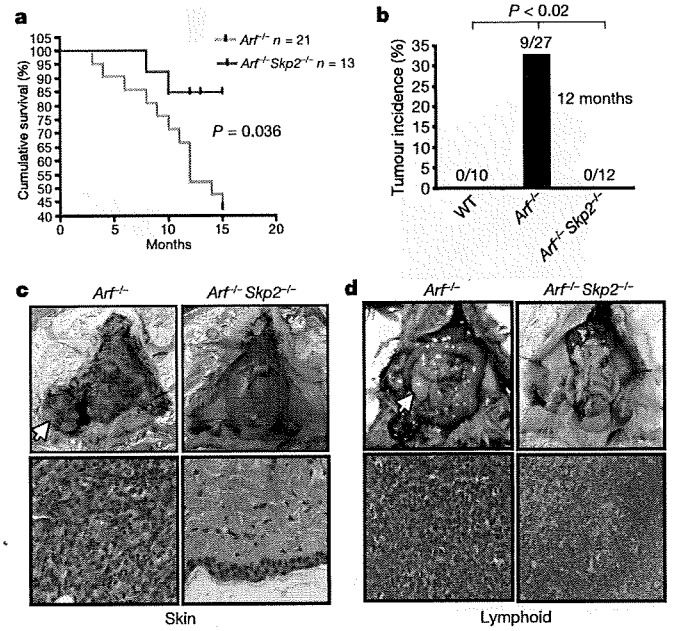

Figure 4 | *Skp2* inactivation restricts tumorigenesis upon *Arf* deficiency. **a**, Kaplan–Meier plot analysis of cumulative survival of $Arf^{-/-}$ and $Arf^{-/-}$ $Skp2^{-/-}$ mice. **b**, A cohort of wild-type, $Arf^{-/-}$ and $Arf^{-/-}$ $Skp2^{-/-}$ mice were analysed for tumorigenesis within a 1-year period. $Arf^{-/-}$ $Skp2^{-/-}$ mice did not develop any tumour up to 1 year observation. Nine out of twenty-seven $Arf^{-/-}$ mice developed either sarcoma or lymphomas, whereas none of 12 $Arf^{-/-}$ $Skp2^{-/-}$ mice developed tumours. The statistic was analysed by chi-squared test, χ^2. **c**, Histopathological analysis of skin tissues from $Arf^{-/-}$ and $Arf^{-/-}$ $Skp2^{-/-}$ mice at 1 year old. Arrow indicates sarcoma. **d**, Histopathological analysis of lymphoid tissues lymphoid tissues from $Arf^{-/-}$ and $Arf^{-/-}$ $Skp2^{-/-}$ mice at 1 year of age. The arrow indicates lymphoma. Original magnification, ×40 (**c**, **d**).

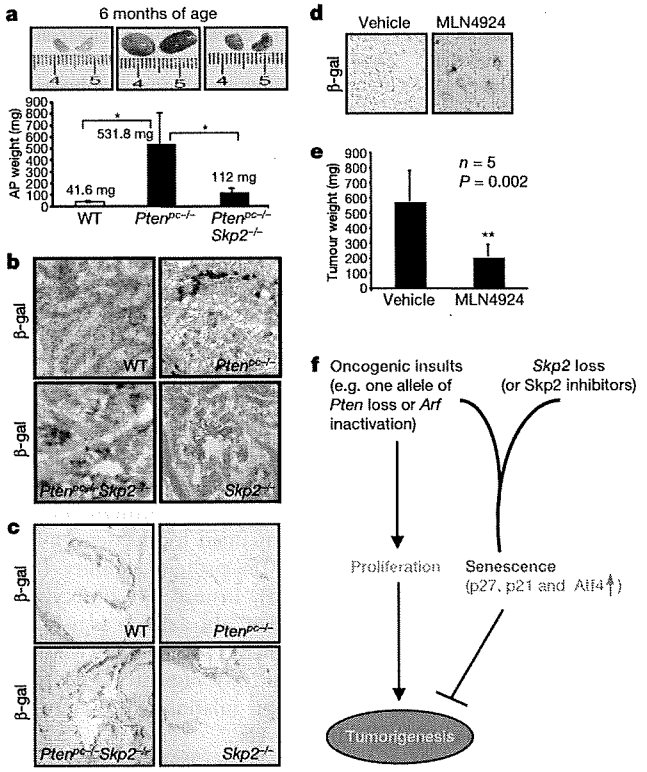

Figure 5 | *Skp2* deficiency restricts prostate cancer development by triggering cellular senescence *in vivo*. **a**, Biopsy of anterior prostate (AP) tumours at 24 weeks from various genotypes of mice and their actual sizes and weights. Results are mean ± s.d. $^*P < 0.05$ using two-tailed Student's *t*-test, $n = 5$. **b**, **c**, Senescence analysis of anterior prostate from $Pten^{pc-/-}$ and $Pten^{pc-/-}$ $Skp2^{-/-}$ mice aged 3 months (**b**) or 15 months (**c**). A representative section from three mice is presented for each genotype. Original magnifications, ×40 (**b**) and ×20 (**c**). **d**, PC3 cells were treated with vehicle or 0.1 μM MLN4924 for 4 days and collected for cellular senescence assay. **e**, Nude mice bearing PC3 xenograft tumours (around 300 mm^3) were treated with vehicle or MLN492, and tumour weight was measured. **f**, Working model for tumour-suppressive cellular senescence driven by oncogenic insults and *Skp2* deficiency.

(Supplementary Fig. 15c). *Skp2* deficiency profoundly enhanced cellular senescence upon *Pten* inactivation (Fig. 5b). This was observed at earlier time points and inversely correlated with cell proliferation (Supplementary Fig. 16a, b). Notably, this response was also sustained over time. We could detect massive β-gal positivity in prostates from $Pten^{pc-/-}$ $Skp2^{-/-}$ mice even at 15 months of age, whereas β-gal positivity was barely detected at that age in prostates from $Pten^{pc-/-}$ mice (Fig. 5c). Thus, *Skp2* inactivation potentiates and sustains over time the senescence response elicited by an oncogenic stimulus, suggesting that pharmacological inhibition of Skp2 may be used as a powerful pro-senescence approach for cancer therapy and chemoprevention.

Skp2–SCF complex inactivation triggers senescence

To corroborate the potential use of such an approach for cancer therapy, we determined whether pharmacological inactivation of the Skp2–SCF complex induces cellular senescence in p53-deficient cells and, importantly, suppresses the growth of the pre-formed tumours. To this end, we took advantage of MLN4924 (ref. 36)—an inhibitor for the neddylation of cullin 1, which is a component of Skp2–SCF complex. We used PC3 prostate cancer cells for this preclinical analysis because these cells are both p53-null and Pten-null, hence representing one of the most aggressive genetic states encountered in human cancer. Remarkably, treatment of MLN4924 in PC3 cells triggered cellular senescence (Fig. 5d). Moreover, the growth of PC3 tumours treated with MLN4924 *in vivo* was also suppressed (Fig. 5e). Coherent with these findings, *Skp2* silencing in PC3 and in DU145 prostate cancer cells, which have also evaded the p53 response, triggered cellular senescence and cooperated with the DNA-damaging agent doxorubicin to induce cellular senescence and growth arrest (Supplementary Fig. 17). These results demonstrate the critical role of Skp2 inactivation in the induction of cellular senescence not only in mouse cells, but also in human cancer cells experiencing failure of p53 and other major tumour-suppressive networks.

Discussion

On the basis of our results, we propose a working model for the role of *Skp2* inactivation-induced cellular senescence in tumour prevention and suppression *in vivo* (Fig. 5f). This model rests on three new and unexpected findings with important therapeutic implications. First, *Skp2* inactivation does not trigger cellular senescence *in vivo* or *in vitro* on its own, but rather elicits a senescence response after oncogenic stress. This response is critically dependent on p27, p21 and Atf4 induction. Our results are supported by recent reports showing that acute inactivation of the von Hippel–Lindau (VHL) tumour suppressor *in vitro* or overexpression of the human T-lymphotropic virus type 1 (HTLV-1) Tax triggers Skp2 downregulation and cellular senescence[37,38]. Second, we show that cellular senescence driven by *Skp2* inactivation along with oncogenic insults takes place without the activation of the $p19^{Arf}$–p53 failsafe pathway. Although senescence is also observed in p53/Pten-null cells such as PC3, it will be important to determine the specific genetic states that favour evasion of this failsafe mechanism, also in a cell-type-specific manner. For instance, loss or constitutively low expression of p27, p21 and Atf4 could impair this response. This knowledge will in turn identify new pharmacological nodes of tumour-type-specific intervention. Third, we show that *Skp2* deficiency in conjunction with oncogenic signals elicits a senescence response that profoundly restricts tumorigenesis *in vivo* in numerous mouse models in which tumour suppressor networks are faulty or inactive. Our findings are consistent with a recent report demonstrating that mice transplanted with BCR–ABL-transduced $Skp2^{-/-}$ bone marrow cells show a delayed onset of a myeloproliferative syndrome[39].

As Skp2 can in principle be subjected to specific pharmacological inhibition because of its enzymatic activity, our results call for the development and optimization of Skp2 small molecule inhibitors. Skp2 pharmacological inhibition could be particularly appealing and effective in view of the fact that complete Skp2 inactivation in the mouse is compatible with life, whereas cellular senescence is only triggered by Skp2 inactivation in conjunction with oncogenic conditions.

METHODS SUMMARY

$Pten^{loxP/loxP}$, $Arf^{-/-}$ and $Skp2^{-/-}$ mice were generated as described previously[2,18,35]. Female $Pten^{loxP/loxP}$ mice were crossed with male *PB-Cre4* transgenic mice for the prostate-specific deletion of *Pten*. MEFs from wild-type and $Skp2^{-/-}$ mice were prepared as previously described[40,41] and cultured in DMEM containing 10% FBS. Cellular senescence was determined by assessing SA-β-gal activity, and the *in vivo* cell proliferation assay was performed by Ki67 staining on the paraffin tissue sections. The cell transformation assay was determined by the soft agar assay. *p53* shRNA is from S. W. Lowe and the pBabe-p53 dominant-negative construct is a gift from M. Oren. MLN4924 was obtained from Millennium Pharmaceuticals.

Full Methods and any associated references are available in the online version of the paper at www.nature.com/nature.

Received 9 October 2009; accepted 11 January 2010.

1. Sharpless, N. E. & DePinho, R. A. Cancer: crime and punishment. *Nature* **436,** 636–637 (2005).
2. Chen, Z. *et al.* Crucial role of p53-dependent cellular senescence in suppression of Pten-deficient tumorigenesis. *Nature* **436,** 725–730 (2005).
3. Xue, W. *et al.* Senescence and tumour clearance is triggered by p53 restoration in murine liver carcinomas. *Nature* **445,** 656–660 (2007).
4. Ventura, A. *et al.* Restoration of p53 function leads to tumour regression *in vivo*. *Nature* **445,** 661–665 (2007).
5. Braig, M. *et al.* Oncogene-induced senescence as an initial barrier in lymphoma development. *Nature* **436,** 660–665 (2005).
6. Michaloglou, C. *et al.* BRAFE600-associated senescence-like cell cycle arrest of human naevi. *Nature* **436,** 720–724 (2005).
7. Collado, M. *et al.* Tumour biology: senescence in premalignant tumours. *Nature* **436,** 642 (2005).
8. Cantley, L. C. & Neel, B. G. New insights into tumor suppression: PTEN suppresses tumor formation by restraining the phosphoinositide 3-kinase/AKT pathway. *Proc. Natl Acad. Sci. USA* **96,** 4240–4245 (1999).
9. Di Cristofano, A. & Pandolfi, P. P. The multiple roles of PTEN in tumor suppression. *Cell* **100,** 387–390 (2000).
10. Salmena, L., Carracedo, A. & Pandolfi, P. P. Tenets of PTEN tumor suppression. *Cell* **133,** 403–414 (2008).
11. Bloom, J. & Pagano, M. Deregulated degradation of the cdk inhibitor p27 and malignant transformation. *Semin. Cancer Biol.* **13,** 41–47 (2003).
12. Nakayama, K. I. & Nakayama, K. Regulation of the cell cycle by SCF-type ubiquitin ligases. *Semin. Cell Dev. Biol.* **16,** 323–333 (2005).
13. Gstaiger, M. *et al.* Skp2 is oncogenic and overexpressed in human cancers. *Proc. Natl Acad. Sci. USA* **98,** 5043–5048 (2001).
14. Latres, E. *et al.* Role of the F-box protein Skp2 in lymphomagenesis. *Proc. Natl Acad. Sci. USA* **98,** 2515–2520 (2001).
15. Shim, E. H. *et al.* Expression of the F-box protein SKP2 induces hyperplasia, dysplasia, and low-grade carcinoma in the mouse prostate. *Cancer Res.* **63,** 1583–1588 (2003).
16. Lin, H. K. *et al.* Phosphorylation-dependent regulation of cytosolic localization and oncogenic function of Skp2 by Akt/PKB. *Nature Cell Biol.* **11,** 420–432 (2009).
17. Chiarle, R. *et al.* S-phase kinase-associated protein 2 expression in non-Hodgkin's lymphoma inversely correlates with p27 expression and defines cells in S phase. *Am. J. Pathol.* **160,** 1457–1466 (2002).
18. Nakayama, K. *et al.* Targeted disruption of *Skp2* results in accumulation of cyclin E and $p27^{Kip1}$, polyploidy and centrosome overduplication. *EMBO J.* **19,** 2069–2081 (2000).
19. Lin, A. W. *et al.* Premature senescence involving p53 and p16 is activated in response to constitutive MEK/MAPK mitogenic signaling. *Genes Dev.* **12,** 3008–3019 (1998).
20. Serrano, M., Lin, A. W., McCurrach, M. E., Beach, D. & Lowe, S. W. Oncogenic *ras* provokes premature cell senescence associated with accumulation of p53 and $p16^{INK4a}$. *Cell* **88,** 593–602 (1997).
21. Kim, W. Y. & Sharpless, N. E. The regulation of INK4/ARF in cancer and aging. *Cell* **127,** 265–275 (2006).
22. Yaswen, P. & Campisi, J. Oncogene-induced senescence pathways weave an intricate tapestry. *Cell* **128,** 233–234 (2007).
23. Hemann, M. T. *et al.* An epi-allelic series of p53 hypomorphs created by stable RNAi produces distinct tumor phenotypes *in vivo*. *Nature Genet.* **33,** 396–400 (2003).
24. Gottlieb, E., Haffner, R., von Ruden, T., Wagner, E. F. & Oren, M. Down-regulation of wild-type p53 activity interferes with apoptosis of IL-3-dependent hematopoietic cells following IL-3 withdrawal. *EMBO J.* **13,** 1368–1374 (1994).
25. Chen, Z. *et al.* Differential p53-independent outcomes of $p19^{Arf}$ loss in oncogenesis. *Sci. Signal.* **2,** ra44 (2009).
26. Bartkova, J. *et al.* Oncogene-induced senescence is part of the tumorigenesis barrier imposed by DNA damage checkpoints. *Nature* **444,** 633–637 (2006).

27. Di Micco, R. *et al.* Oncogene-induced senescence is a DNA damage response triggered by DNA hyper-replication. *Nature* **444,** 638–642 (2006).
28. Mallette, F. A., Gaumont-Leclerc, M. F. & Ferbeyre, G. The DNA damage signaling pathway is a critical mediator of oncogene-induced senescence. *Genes Dev.* **21,** 43–48 (2007).
29. Yu, Z. K., Gervais, J. L. & Zhang, H. Human CUL-1 associates with the SKP1/SKP2 complex and regulates $p21^{CIP1/WAF1}$ and cyclin D proteins. *Proc. Natl Acad. Sci. USA* **95,** 11324–11329 (1998).
30. Denoyelle, C. *et al.* Anti-oncogenic role of the endoplasmic reticulum differentially activated by mutations in the MAPK pathway. *Nature Cell Biol.* **8,** 1053–1063 (2006).
31. Kim, I., Xu, W. & Reed, J. C. Cell death and endoplasmic reticulum stress: disease relevance and therapeutic opportunities. *Nature Rev. Drug Discov.* **7,** 1013–1030 (2008).
32. Di Cristofano, A. *et al.* Impaired Fas response and autoimmunity in $Pten^{+/-}$ mice. *Science* **285,** 2122–2125 (1999).
33. Di Cristofano, A., Pesce, B., Cordon-Cardo, C. & Pandolfi, P. P. Pten is essential for embryonic development and tumour suppression. *Nature Genet.* **19,** 348–355 (1998).
34. Kamijo, T., Bodner, S., van de Kamp, E., Randle, D. H. & Sherr, C. J. Tumor spectrum in ARF-deficient mice. *Cancer Res.* **59,** 2217–2222 (1999).
35. Kamijo, T. *et al.* Tumor suppression at the mouse *INK4a* locus mediated by the alternative reading frame product $p19^{ARF}$. *Cell* **91,** 649–659 (1997).
36. Soucy, T. A. *et al.* An inhibitor of NEDD8-activating enzyme as a new approach to treat cancer. *Nature* **458,** 732–736 (2009).
37. Young, A. P. *et al.* VHL loss actuates a HIF-independent senescence programme mediated by Rb and p400. *Nature Cell Biol.* **10,** 361–369 (2008).
38. Kuo, Y. L. & Giam, C. Z. Activation of the anaphase promoting complex by HTLV-1 tax leads to senescence. *EMBO J.* **25,** 1741–1752 (2006).
39. Agarwal, A. *et al.* Absence of SKP2 expression attenuates BCR-ABL-induced myeloproliferative disease. *Blood* **112,** 1960–1970 (2008).
40. Lin, H. K., Bergmann, S. & Pandolfi, P. P. Cytoplasmic PML function in TGF-β signalling. *Nature* **431,** 205–211 (2004).
41. Yang, W. L. *et al.* The E3 ligase TRAF6 regulates Akt ubiquitination and activation. *Science* **325,** 1134–1138 (2009).

Supplementary Information is linked to the online version of the paper at www.nature.com/nature.

Acknowledgements We are grateful to C. J. Sherr, S. W. Lowe and M. Oren for mice and reagents. We would also like to thank B. Carver, L. DiSantis, J. Clossey and S. Megan for editing and critical reading of the manuscript, J. A. Koutcher, C. Le, C. Matei and M. Lupa for MRI analysis, as well all the members of the Pandolfi laboratory for comments and discussion. We extend our thanks to M. Rolfe, P. G. Smith, and Millennium Pharmaceuticals for discussion and for providing the MLN4924 compound. This work was supported by NIH grants to P.P.P. and M.D. Anderson Trust Scholar Award and DOD Prostate Cancer New Investigator Award to H.K.L.

Author Contributions H.K.L. and P.P.P. designed the experiments and wrote the manuscript; H.-K.L., Z.C., G.W., S.-W.L., C.N., C.-H.C., W.-L.Y., J.W. and A.E. performed the experiments; C.C.-C. and J.T-F. performed the histopathological analysis of the mice; K.I.N. provided the $Skp2^{-/-}$ mice.

Author Information Reprints and permissions information is available at www.nature.com/reprints. The authors declare no competing financial interests. Correspondence and requests for materials should be addressed to P.P.P. (ppandolf@bidmc.harvard.edu).

METHODS

shRNA-mediated silencing. For the retrovirus-infection system, *p27* shRNA (5′-GTGGAATTTCGACTTTCAG-3′), *Atf4* shRNA (5′-GAGCATTCCTTTAG TTTAG-3′), and GFP shRNA (5′-GCAAGCTGACCCTGAAGTTC-3′) were subcloned into the pSUPER-puro vector (Oligoengine) according to standard procedures and transfected into Phoenix packaging cells. For lentiviral shRNA infection, 293T cells were co-transfected with *p27*, *Atf4*, *p21*, *Skp2* or GFP control shRNA along with packing plasmids (ΔVPR8.9) and envelope plasmid (VSV-G) using Lipofectamine 2000 reagents according to the manufacturer's instructions. *Skp2*-lentivivral shRNA-1 (5′-GATAGTGTCATGCTAAAGAAT-3′), *p27*-lentivivral shRNA-1 (5′-CGCAAGTGGAATTTCGACTTT-3′), *p27*-lentivivral shRNA-2 (5′-CCCGGTCAATCATGAAGAACT-3′), *Atf4*-lentivivral shRNA-1 (5′-GCGAG TGTAAGGAGCTAGAAA-3′), *Atf4*-lentivivral shRNA-2 (5′-CGGACAAAGATA CCTTCGAGT-3′), *p21*-lentivivral shRNA-1 (5′ CTGGTGTCTGAGCGGCCT GAA-3′), *p21*-lentivivral shRNA-2 (5′-GACAGATTTCTATCACTCCAA-3′), and GFP shRNA (5′-GCAAGCTGACCCTGAAGTTC-3′) were transfected with packing plasmids into 293T cells for 2 days, and virus particles containing *p27*, *p21*, *Atf4*, *Skp2* or GFP shRNA were used to infect mammalian cells. All the infected cells were cultured in a medium containing the appropriate antibiotics.

Western blot analysis and immunohistochemistry. Cell lysates were prepared with RIPA buffer (PBS, 1% Nonidet P40, 0.5% sodium deoxycholate, 0.1% SDS and protease inhibitor cocktail (Roche)). The following antibodies were used for western blot analysis: anti-$p19^{Arf}$ (NeoMarkers), anti-p53 (Novocastra), anti-p21 (Santa Cruz), anti-β-actin (Sigma), anti-Hsp90 (BD transduction laboratories), anti-p27 (BD transduction laboratories), anti-α-tubulin (Sigma), anti-phospho-p53 (Ser15) (Cell Signaling), anti-phospho-H2ax (Ser139) (Cell Signaling), anti-phospho-eIF2α (Ser51) (Cell Signaling), anti-eIF2α (Cell Signaling), anti-phospho-Perk (Thr980) (Cell Signaling), anti-cyclin D1 (Santa Cruz), anti-E2F1 (Santa Cruz), anti-Cdt1 (Proteintech Group), anti-Ras (Oncogene), anti-E1A (Neomarkers), and anti-Atf4 (Santa Cruz). For immunohistochemistry, tissues were fixed in 10% formalin and embedded in paraffin in accordance with standard procedures. Sections were stained with anti-p27 (BD transduction laboratories), anti-Ki67 (Novocastra), anti-Pten (Neomarkers) and anti-p53 (Novocastra) antibodies.

Cell proliferation, transformation and senescence. Primary MEFs were isolated from individual embryos of various genotype at passage 2, infected with retroviruses or lentiviruses expressing GFP shRNA, *p27* shRNA or *Atf4* shRNA for 2 days, selected with 2 $\mu g\,ml^{-1}$ puromycin for 4 days, and plated for the cell proliferation and senescence assay. For cell proliferation assay, 2×10^4 MEFs were seeded in 12 wells in triplicate, collected, and stained with trypan blue at different days. Numbers of viable cells were directly counted under the microscope. To determine cellular senescence, MEFs were plated at 10^4 cells per well of a 6-well plate in triplicate, and after 4 days SA-β-gal activity was measured using the senescence detection kit (Calbiochem) and quantified (around 100–200 cells per well). For *in vivo* cellular senescence, frozen sections 6-μm thick were stained for β-gal as described earlier. For *in vivo* cell proliferation, the paraffin section was used for Ki67 staining, and the percentages of Ki67-positive cells (around 500 cells) from each sample were counted. For transformation assay, wild-type and $Skp2^{-/-}$ MEFs (3×10^4) infected with Ras(G12V) and E1A were suspended in a medium containing 0.3% agar onto solidified 0.6% agar per well of a 6-well plate, and the number of colonies was counted after 21 days.

Apoptosis assay. Primary MEFs of various genotypes of mouse embryos were cultured in 10% FBS for 2 days; cells were collected and labelled with Annexin-V–FITC, followed by a flow cytometry analysis.

MRI. Individual mice were subjected to MRI assessment for the detection of prostate tumours as described[42].

***In vivo* drug treatment in the preclinical tumour model.** Nude mice bearing PC3 xenograft tumours (around 300 mm^3) were treated with vehicle or 90 $mg\,kg^{-1}$ MLN492. Tumour weight was measured at the time of collection after 15 days of treatment with a scheduling regimen of 3 days of treatment followed by 3 days without treatment for a total of three courses.

42. Chen, Z. *et al.* Crucial role of p53-dependent cellular senescence in suppression of Pten-deficient tumorigenesis. *Nature* **436**, 725–730 (2005).